Modal Techniques for Remote Identification of Nonlinear Reactions at Gap-Supported Tubes Under Turbulent Excitation

Xavier Delaune

Laboratoire d'Études de Dynamique,
Commissariat à l'Énergie Atomique,
CEA, DEN, DM2S, SEMT,
F-91191 Gif-sur-Yvette, France
e-mail: xavier.delaune@cea.fr

José Antunes

e-mail: jantunes@itn.pt

Vincent Debut

Applied Dynamics Laboratory,
Instituto Tecnológico e Nuclear,
ITN/ADL, Estrada Nacional 10,
2686 Sacavem Codex, Portugal

Philippe Piteau

Laurent Borsoi

Laboratoire d'Études de Dynamique,
Commissariat à l'Énergie Atomique,
CEA, DEN, DM2S, SEMT,
F-91191 Gif-sur-Yvette, France

Predictive computation of the nonlinear dynamical responses of gap-supported tubes subjected to flow excitation has been the subject of very active research. Nevertheless, experimental results are still very important, for validation of the theoretical predictions as well as for asserting the integrity of field components. Because carefully instrumented test tubes and tube-supports are seldom possible, due to space limitations and to the severe environment conditions, there is a need for robust techniques capable of extracting, from the actual vibratory response data, information that is relevant for asserting the components integrity. The dynamical contact/impact (vibro-impact) forces are of paramount significance, as are the tube/support gaps. Following our previous studies in this area using wave-propagation techniques (De Araújo, Antunes, and Piteau, 1998, "Remote Identification of Impact Forces on Loosely Supported Tubes: Part 1—Basic Theory and Experiments," J. Sound Vib., 215, pp. 1015–1041; Antunes, Paulino, and Piteau, 1998, "Remote Identification of Impact Forces on Loosely Supported Tubes: Part 2—Complex Vibro-Impact Motions," J. Sound Vib., 215, pp. 1043–1064; Paulino, Antunes, and Izquierdo, 1999, "Remote Identification of Impact Forces on Loosely Supported Tubes: Analysis of Multi-Supported Systems," ASME J. Pressure Vessel Technol., 121, pp. 61–70), we apply modal methods in the present paper for extracting such information. The dynamical support forces, as well as the vibratory responses at the support locations, are identified from one or several vibratory response measurements at remote transducers, from which the support gaps can be inferred. As for most inverse problems, the identification results may prove quite sensitive to noise and modeling errors. Therefore, topics discussed in the paper include regularization techniques to mitigate the effects of nonmeasured noise perturbations. In particular, a method is proposed to improve the identification of contact forces at the supports when the system is excited by an unknown distributed turbulence force field. The extensive identification results presented are based on realistic numerical simulations of gap-supported tubes subjected to flow turbulence excitation. We can thus confront the identified dynamical support contact forces and vibratory motions at the gap-support with the actual values stemming from the original nonlinear computations. The important topic of dealing with the imperfect knowledge of the modal parameters used to build the inverted transfer functions is thoroughly addressed elsewhere (Debut, Delaune, and Antunes, 2009, "Identification of Nonlinear Interaction Forces Acting on Continuous Systems Using Remote Measurements of the Vibratory Responses," Proceedings of the Seventh EUROMECH Solids Mechanics Conference (ESMC2009), Lisbon, Portugal, Sept. 7–11). Nevertheless, identifications are performed in this paper based on both the exact modes and also on randomly perturbed modal parameters. Our results show that, for the system addressed here, deterioration of the identifications is moderate when realistic errors are introduced in the modal parameters. In all cases, the identified results compare reasonably well with the real contact forces and motions at the gap-supports. [DOI: 10.1115/1.4001077]

1 Introduction

Flow-induced vibrations of heat-exchanger tube bundles and nuclear fuel rods are a major source of concern, when component life and plant availability are addressed. Excitation by the flow turbulence and possible fluid-elastic phenomena may lead to a premature failure of the components due to material fatigue or to vibro-impact wear of the gap-supported tubes. Hence, the authors and other researchers have developed predictive methods and computer codes to analyze heat-exchanger tube responses and wear, for realistic multisupported tubes and flow configurations, with considerable success [1–7], as attested by validation of the predictive techniques achieved through laboratory experiments [8–11].

Experimental work on vibro-impacting tubes calls for carefully instrumented test tubes and tube-supports—see, for instance, Ref. [12]. Such ideal conditions are often, although not always, possible for laboratory experiments. But they are seldom feasible when addressing real field components, due to space limitations and to the severe environment conditions (temperature, radiation), which prevent an adequate instrumentation of the tube-supports. Therefore, typically, the tube/support impact forces cannot be directly monitored under real operating conditions. Then, identification techniques that enable the diagnosis of tube/support interac-

tion, based on remote vibratory measurements, become quite valuable—for validating the predictive methods, as well as for condition-monitoring of the real components.

Vibro-impact problems are severely nonlinear and, whenever the system responses are unknown (as typically is the case for predictive analysis), must be dealt using costly computational approaches. One should notice however that if the nonlinear system dynamical responses are known (either from measurements or from previous computations), then the *inverse problem* of identifying the excitations (including all nonlinear interaction forces) from the available responses becomes *linear* because the basic vibrating system can be modeled as such. In other words, once the system response is available, then even the motion-dependent forces (such as impacts) can be seen as common external excitations, which led to the measured tube responses. This fact is of great significance, when addressing the inverse problem of impact force identification, either from measured of simulated vibro-impact responses.

Previous work in this field includes papers by Whiston and co-worker [13,14], who discussed theoretical and experimental aspects related to the remote identification of impact forces. These authors modeled the flexural propagation waves in the frequency domain using a Timoshenko beam model without damping. In his book and in a series of related papers, Doyle [15] followed a similar approach. These authors also presented satisfactory experimental results provided by single impacts acting on long beams, in such a way that wave reflections at the boundaries do not interfere seriously with the direct wave used for identification proposes. In a series of papers [16–18], using small arrays of motion transducers, the present authors further extended wave-propagation techniques, based on a simple Bernoulli–Euler beam formulation, in order to deal effectively with the wave reflections, which arise at the boundary conditions of finite-length beams.

Lin and Bapat [19,20] presented methods for estimation of the impact forces and the support gap in a single-degree-of-freedom system, respectively, for sinusoidal and random excitations. The extension of these methods to a beam with a single nonlinear gap-support was proposed by using a modal approach in the frequency domain [21]. Busby and Trujillo [22] presented a similar approach, in which the force identification is achieved in the time domain. The extension of these methods to multisupported beams, which display ill-defined or even unknown modal basis, seems problematic. Nevertheless, our experimental work [18] performed on a beam with three gap-supports provided high quality force identifications, provided that vibro-impacts arise at all intermediate gap-supports (e.g., with no preload effects at intermediate supports). Wu and Yeh [23] discussed the problem of source separation, for several simultaneous impacts, using a time-domain approach. The so-called cepstral methods of deconvolution, which may be quite useful when dealing with nondispersive phenomena, have been used very seldom for dispersive flexural waves [24]. In a recent paper, Inoue et al. [25] reviewed several techniques for the identification of impact forces using inverse methods.

Most of the basic work on inverse theory was triggered by identification problems in the geophysics/astrophysics and radar/sonar research fields. These problems usually involve nondispersive phenomena, and lead to problems somewhat different from those of concern here. Nevertheless, for an approach to inverse problems, useful information will be found in the applied work by Jeffrey and Rosner [26], Dimri [27], and Parker [28]. In a more general context, Press et al. [29], Groetch [30], and Hansen [31] offered excellent reviews on inverse problems and current methods for solving them.

The main difficulty with inverse problems is ill-conditioning—physical or numerical—of the transfer/propagation operators, which describe the phenomena. This leads to inverse formulations which are very sensitive to noise contamination of the measured signals. Problems may be partially overcome by regularization of the transformation operators, by using several methods, namely,

singular value decomposition, incorporation of physical constraints, and optimization techniques [16,29–32]. In the context of vibro-impact system identification, ill-conditioning difficulties are enhanced due to the dispersive nature of flexural waves.

The present paper follows our previous work on remote vibro-impact identification using wave-propagation techniques [16–18]. Here, we explore the use of modal techniques for extracting—from one or several vibratory response measurements at remote locations—the dynamical support forces as well as the vibratory responses at the support locations, from which the support gaps may be inferred. Both techniques work in the frequency domain. In contrast to the wave-propagation approach, the modal approach asks for a larger number of parameters in order to describe the system dynamics matrices $H(\omega)$ to be inverted, which is certainly a disadvantage. Indeed, while only a couple of parameters related to the wave speed and dissipation are needed to describe propagation in the $k(\omega)$ dispersion equation, the modal approach needs all the modal parameters m_n, ω_n, ζ_n, and $\varphi_n(x)$, $n = 1, 2, \ldots, N$ in the frequency range of interest. However, wave-propagation techniques must cope with a multitude of reflected waves stemming from the boundary conditions of finite-length beams, while these effects are automatically encapsulated in the modal parameters, a fact that significantly favors identification techniques based on the modal formulation.

Topics discussed in the paper include regularization methods to mitigate the effects of nonmeasured noise perturbations. As a significant feature, a method is proposed to improve the identification of contact forces at the supports when the system is excited by an unknown distributed turbulence force field. Such approach proves particularly valuable when addressing the nonimpulsive contact forces at preloaded intermediate supports. The extensive identifications presented here are based on realistic numerical simulations of gap-supported tubes subjected to flow turbulence excitation. We can thus confront the identified dynamical support contact forces and vibratory motions at the gap-support with the actual values stemming from the original nonlinear computations.

The important topic of dealing with the imperfect knowledge of the modal parameters used to build the inverted transfer functions is addressed elsewhere [32,33], where we show that optimization techniques can effectively improve an initial estimate of the modal parameters, in order to obtain better estimates suitable for the inversion problem. Nevertheless, identifications are performed in this paper based both on the exact modal basis and also on randomly perturbed modes. We thus simulate the effects of incertitude in the knowledge of all modal parameters—m_n, ω_n, ζ_n and $\varphi_n(x)$. The results obtained show that the problem addressed in this paper is tolerant enough to realistic errors in the modal parameters. Actually, the deterioration of the identified contact forces and displacements, when errors are introduced in the modal parameters, is nearly masked by the residual deterioration due to the unmeasured turbulence excitation. In all cases, the identification results obtained for this system seem accurate enough for practical purposes.

2 Vibrations of Gap-Supported Tubes Excited by Flow Turbulence

2.1 Time-Domain Computation of the Nonlinear Dynamics. As discussed in Ref. [16], the simple Bernoulli–Euler theory for flexural vibrations proved to be adequate for impact identification. Therefore, assuming a viscous damping model, the small-amplitude flexural response of a tube with constant cross-sectional properties is described by the differential equation:

$$\rho A \frac{\partial^2 y}{\partial t^2} + \eta \frac{\partial y}{\partial t} + EI \frac{\partial^4 y}{\partial x^4} = f(x,t) \tag{1}$$

where $f(x,t)$ is the total external excitation field, $y(x,t)$ is the transverse vibratory response, E is Young's modulus, ρ is the mass density of the tube, A is the area, I is the moment of inertia of the

cross section, while η is a viscous dissipation coefficient.

As amply documented in Refs. [2–4,12], the vibro-impact non-linear computations may be performed in an effective manner by projecting Eq. (1) on the tube modes (unconstrained at the non-linear support locations). Then, the following discretized modal equations are obtained:

$$m_n \ddot{q}_n + 2 m_n \omega_n \zeta_n \dot{q}_n + m_n \omega_n^2 q_n = f_n(t) = f_n^T(t) + f_n^C(t) \quad (2)$$

in terms of the modal amplitudes $q_n(t)$ and its derivatives, with $n = 1, 2, \ldots, N$. The physical motions may be computed from the modal responses at any time and location, by modal superposition

$$y(x,t) = \sum_{n=1}^{N} \varphi_n(x) q_n(t) \quad (3)$$

and similarly for all time-derivatives. The computational truncation index N of the modal basis is chosen accounting for the various sources of excitation—here, the distributed turbulence force field $f_T(x,t)$ and the localized contact/impact forces $F_C(t)$ at the gap-support location x_C (a single gap-support will be assumed in this work), which lead to the modal forces

$$f_n^T(t) = \int_0^L f_T(x,t) \varphi_n(x) dx \quad (4)$$

$$f_n^C(t) = \int_0^L F_C(t) \delta(x - x_C) \varphi_n(x) dx = F_C(t) \varphi_n(x_C) \quad (5)$$

Modeling of the time-domain turbulence forces is performed as thoroughly explained by Antunes and co-workers [33,34]. A set of uncorrelated point forces applied along the tube is generated, using a simple method that preserves the frequency content as well as the overall space correlation of the original turbulence field. On the other hand, the contact force $F_C(t)$ at the nonlinear gap-support is computed in an explicit manner from the system response, at each time-step, using the following penalty formulation:

$$F_C(t) = \begin{cases} -K_C[y(x_C,t) - \delta_C] & \text{if } |y(x_C,t)| > \delta_C \\ 0 & \text{if } |y(x_C,t)| < \delta_C \end{cases} \quad (6)$$

where K_C is a suitable value for the contact stiffness at the support and δ_C is the support gap. One may notice, from Eqs. (3) and (6), that the tube/support interaction couples the system unconstrained modes. Indeed, during contact, one obtains

$$F_C(t) = -K_C \left[\sum_{n=1}^{N} \varphi_n(x_C) q_n(t) - \delta_C \right] \quad (7)$$

which clearly shows that the tube/support impacts couple all modes, redistributing the modal energies. Numerical integration of the closed nonlinear system (2)–(6) is achieved using a classic Newmark constant average acceleration algorithm.

2.2 Numerical Simulations of a Gap-Supported Tube. The method described in Sec. 2.1 was used to simulate the nonlinear dynamical responses of a tube excited by the turbulence of a uniform transverse flow. The modeled tube has length $L = 1$ m, diameter $D = 20 \cdot 10^{-3}$ m, and wall thickness $e = 1.5 \cdot 10^{-3}$ m. It is made in steel, with mass density $\rho = 7800$ kg/m³ and Young's modulus $E = 2 \cdot 10^{11}$ Pa. Common pinned boundary conditions are assumed at $x = 0$ and $x = L$, leading to the simple modeshapes $\varphi_n(x) = \sin(n\pi x / L)$.

At $x_C = 0.6$ m, a point-support is modeled using two opposite springs with stiffness $K_C = 10^6$ N/m. Two quite different configurations were simulated: (a) the first one assuming a symmetrical gap $\delta_C = \pm 10^{-3}$ m at the gap-support and no preload, as shown in Fig. 1(a), and (b) in the second configuration a preload of 2N was imposed, which is enough to insure permanent contact between
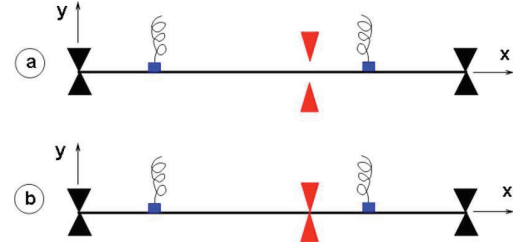

Fig. 1 Configurations used in numerical simulations: beam length $L = 1$ m, support location $x_C = 0.6$ m, response measurement locations $x_1 = 0.21$ m, and $x_2 = 0.77$ m. (a) First configuration with a symmetrical gap $\delta_C = \pm 10^{-3}$ m. (b) Second configuration with permanent contact

the tube and the support (for the turbulent excitation level used in the computations). Then, for all practical purposes, the second configuration behaves linearly, as sketched in Fig. 1(b).

The tube is subjected to a uniform transverse flow with mass density $\rho_f = 1000$ kg/m³ and average velocity $\bar{V}_f = 6$ m/s. The dimensionless equivalent reference spectrum $\Phi_E^{\text{ref}}(f_R)$ of the turbulence forces per unit tube length used in the computations, as a function of the reduced frequency $f_R = fD / \bar{V}_f$ (where f is the frequency in Hertz), is given as

$$\Phi_E^{\text{ref}}(f_R) = \begin{cases} 4 \cdot 10^{-4} \, f_R^{-0.5} & \text{for } f_R < 0.2 \\ 3 \cdot 10^{-6} \, f_R^{-3.5} & \text{for } f_R > 0.2 \end{cases}, \quad f_R = \frac{fD}{\bar{V}_f} \quad (8)$$

with reference parameters $L_{\text{ref}} = 1$ m and $D_{\text{ref}} = 20 \cdot 10^{-3}$ m—see Ref. [4] for details. Figure 2 shows the dimensionless spectrum of Eq. (8), and the corresponding local excitation turbulence spectrum, as computed from [4,34,35]

$$\Phi_T(f) = \left[\frac{1}{2} \rho_f \bar{V}_f^2 D \right]^2 \frac{D}{\bar{V}_f} \Phi_E^{\text{ref}}(f_R) \quad (9)$$

Time-domain computations were performed using a modal basis with 18 flexural modes in the xy plane. Their lowest and highest modal frequencies are 43 and 11568 Hz, respectively. A constant modal damping $\zeta_n = 1\% (\forall n)$ was assumed for all modes. The time-histories of the tube responses (accelerations $A_1(t) \equiv \ddot{y}(x_1,t)$ and $A_2(t) \equiv \ddot{y}(x_2,t)$, velocities $V_1(t) \equiv \dot{y}(x_1,t)$ and $V_2(t) \equiv \dot{y}(x_2,t)$, displacements $D_1(t) \equiv y(x_1,t)$ and $D_2(t) \equiv y(x_2,t)$), respectively at
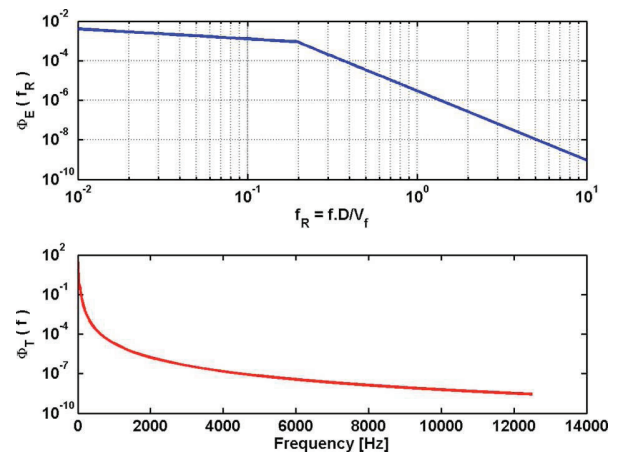

Fig. 2 Dimensionless equivalent reference spectrum $\Phi_E^{\text{ref}}(f_R)$ of the turbulence forces per unit tube length, as a function of the reduced frequency $f_R = fD / \bar{V}_f$, and the corresponding local excitation turbulence spectrum $\Phi_T(f)$
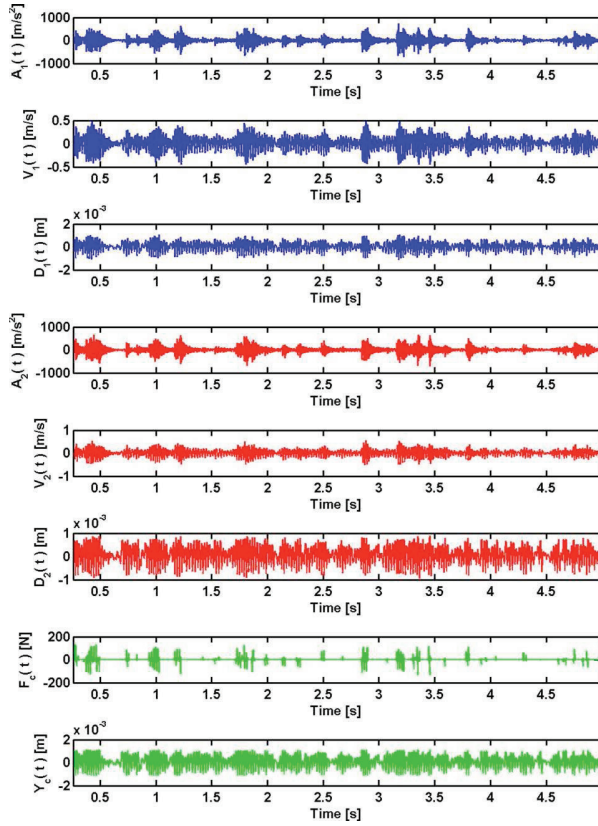
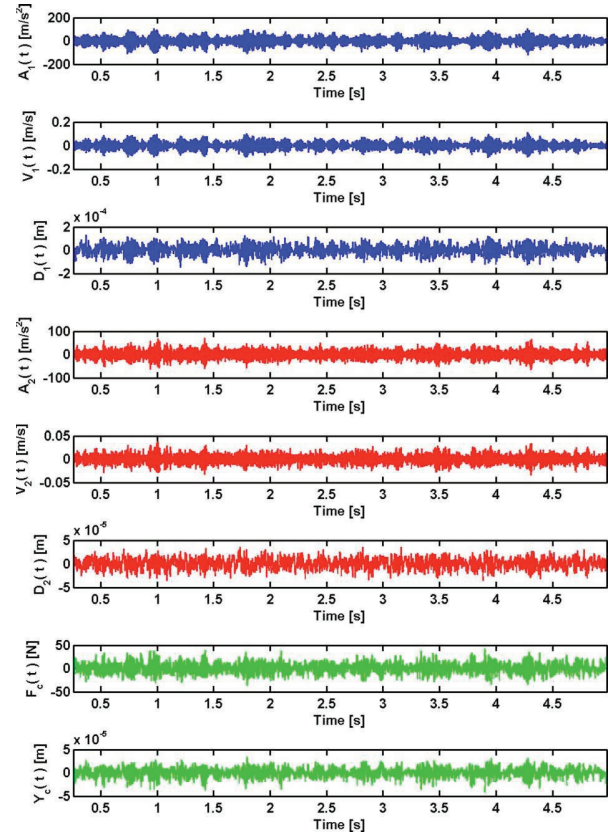**Fig. 3 Tube responses for the gap-support configuration (a)**

Fig. 4 Tube responses for the preload configuration (b)

locations $x_1 = 0.21$ m and $x_2 = 0.77$ m, as well as the contact/impact forces $F_C(t)$ and displacement responses $Y_C(t) \equiv y(x_C, t)$ at the support location $x_C = 0.6$ m, are shown in Figs. 3 and 4. As attested by the different scales of the plots in Figs. 3 and 4, one can notice strong impact forces as well as a significant response amplitude for configuration (a), while the reaction forces and response amplitude at the support location are much lower for the preload configuration (b). The corresponding spectra are shown in Figs. 5 and 6 (configurations a and b, respectively), which highlight the expected increase in high-frequency information for the velocity and acceleration response signals.

This data will be used to perform the remote identifications from $y(x_1, t)$ and $y(x_2, t)$—or their time-derivatives—which will then compared with the true values of $F_C(t)$ and $y(x_C, t)$.

3 Identification Problem Formulation

As pointed earlier, this work is obviously related to a severely nonlinear problem, which in predictive analysis calls for costly computational approaches in order to obtain the dynamical responses. However, as also pointed, if the system nonlinear responses are already known either from measurements or from previous computations, then the inverse problem of identifying the excitations (including all nonlinear interaction forces) from the available responses becomes linear. Then, excitation identification becomes essentially a problem of response deconvolution, when working in the time domain, or—which is more practical—response inversion, by working in the frequency domain. Fourier techniques can be advantageously applied to the inverse problem, and the basic identification procedure for a point excitation $F(x_E, t)$ at location x_E, from a response measurement $y(x_R, t)$ at location x_R, can be summarized as

$$y(x_R, t) \overset{FFT[\ldots]}{\Rightarrow} Y(x_R, \omega) = H(x_E, x_R, \omega) F(x_E, \omega)$$

$$\Rightarrow F(x_E, \omega) = \frac{Y(x_R, \omega)}{H(x_E, x_R, \omega)} \overset{FFT^{-1}[\ldots]}{\Rightarrow} F(x_E, t) \quad (10)$$

where the force identification transfer function is built as usual

$$H^d(x_E, x_R, \omega) = \sum_{n=1}^{N_{\text{ide}}} \frac{\varphi_n(x_E) \varphi_n(x_R)}{m_n[\omega_n^2 - \omega^2 + 2i\omega\omega_n\zeta_n]} \quad (11)$$

for displacement response signals. If velocity or acceleration responses are used, then

$$H^v(x_E, x_R, \omega) = i\omega H^d(x_E, x_R, \omega) \quad (12)$$

$$H^a(x_E, x_R, \omega) = -\omega^2 H^d(x_E, x_R, \omega) \quad (13)$$

This procedure may be generalized to more than one excitation and more than one response measurement, provided the inverse problem is well posed, or that additional information constraints on the interaction forces are available and be included in the formulation.

Equation (10) appears deceptively simple. Actually, as for most inverse problems, identification results prove quite sensitive to noise and modeling errors. Regularization methods must be applied to the inverted transfer function $H(x_E, x_R, \omega)$, in order to overcome the perverse effects of the random noise and/or nonmeasured force perturbations. Here, the perturbing effect comes from the unmeasured distributed turbulence force field.

Figure 7 shows the transfer functions used for inversion, to identify the contact/impact forces $F_C(\omega)$ from the responses $Y(x_1, \omega)$ and $Y(x_2, \omega)$. These transfer functions were built using the exact modal parameters of the beam, those which were used for computing the time-domain vibro-impact responses. However,
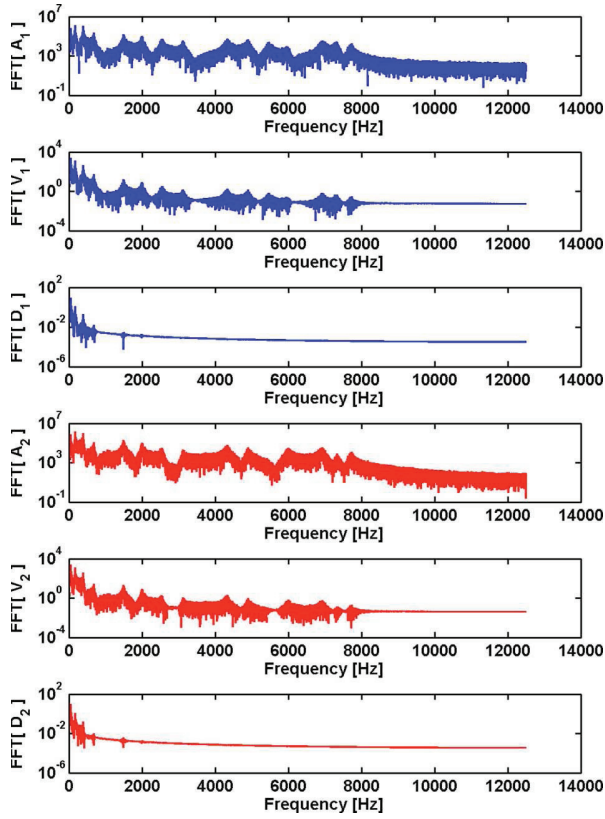
Fig. 5 Response spectra for the gap-support configuration (a)
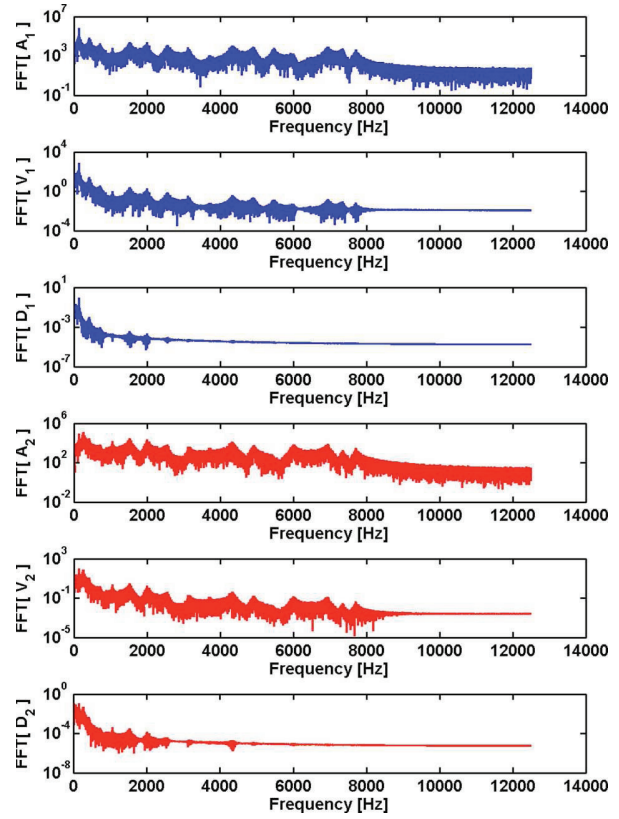

Fig. 6 Response spectra for the preload configuration (b)

because in practice only a subset of the modal basis is usually known, we decided to perform the identification work using only 16 modes. The effect of random perturbations in the modal parameters will be investigated later in the paper. Notice that inversion is most sensitive to noise and unmeasured perturbations in the frequency regions about the antiresonances of the $H(x_C, x_R, \omega)$, which are unduly amplified by the inversion $1/H(x_C, x_R, \omega)$. Figure 8 shows, beyond the real impact force $F_C(t)$, the force identifications $F_{1,2}^a(t)$, $F_{1,2}^v(t)$, and $F_{1,2}^d(t)$, obtained for configuration (a), respectively from $A_{1,2}(t)$, $V_{1,2}(t)$, and $D_{1,2}(t)$, when Eq. (10) is used without precautions. The effects of the unaccounted turbulence forces—which act as a "noise" perturbation—are obvious, in particular concerning the force identifications from the response displacements.

4 Inverse Problem Regularization

Several techniques are available for the regularization of inverse problems. All of them amount to some kind of *filtering*, in order to inhibit the noise amplification—Tikhonov regularization [29–31] being the most common procedure. At this stage we will apply a regularization technique which is both simple to implement in the frequency domain and quite effective. For each transfer function, a regularization parameter ε is introduced, which will act as a lower boundary on $H(x_C, x_R, \omega)$, beyond which filtering of the inverse problem is enabled. In the scheme implemented here, we replace $H(x_C, x_R, \omega)$ in Eq. (10) by a regularized transfer function $H_{\mathrm{REG}}(x_C, x_R, \omega; \varepsilon)$, computed as follows:

$$H_{\mathrm{REG}}(x_C, x_R, \omega; \varepsilon) = \begin{cases} H(x_C, x_R, \omega) & \text{if } |H(x_C, x_R, \omega)| > \varepsilon \\ \varepsilon \dfrac{H(x_C, x_R, \omega)}{|H(x_C, x_R, \omega)|} & \text{if } |H(x_C, x_R, \omega)| < \varepsilon \end{cases}$$

$$(14)$$

Then an obvious issue arises, which is the choice of an optimal value of the filtering parameter ε. If ε is too small, then regularization is negligible and excessively amplified noise is obtained as a result. On the other hand, if ε is too large, then regularization will "drown" the problem physics leading to a large error in the excessively smooth identified result. These arguments motivate
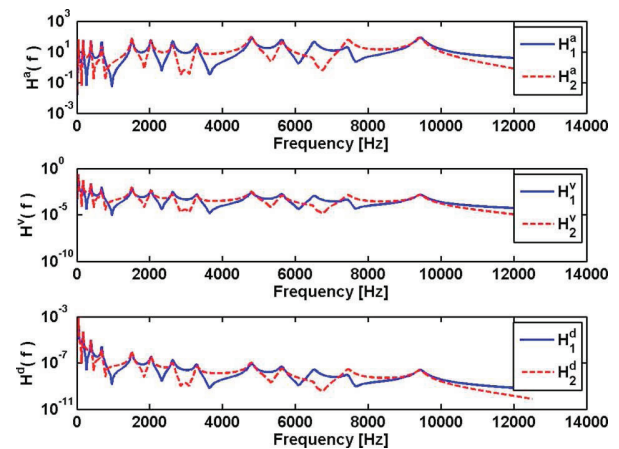

Fig. 7 Transfer functions $H(x_C, x_1, \omega)$ and $H(x_C, x_2, \omega)$ used to compute the impact forces from the acceleration, velocity, and displacement
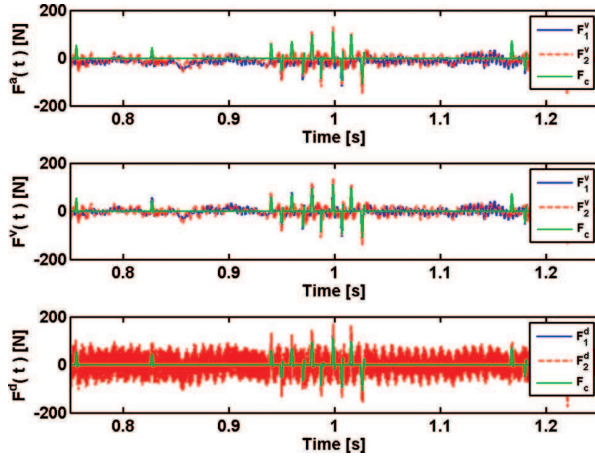
Fig. 8 Nonregularized impact force identification for the gap-support configuration (a)

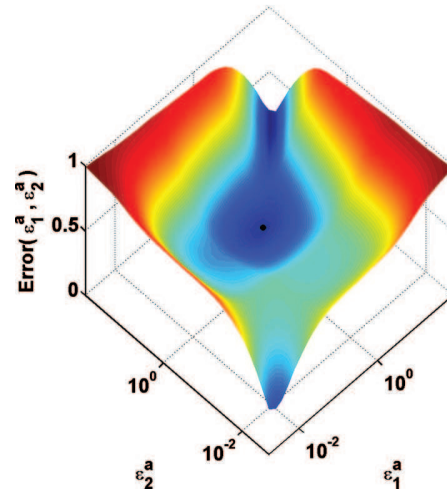Optimal regularisation : $\varepsilon_1^a = 9.85\text{e-}001$, $\varepsilon_2^a = 1.63\text{e+}000$

Fig. 9 Optimal values of the regularization parameters by minimizing the difference between two estimates of the impact force from the acceleration signals

the classical L-curve diagram [29–31] often used, where the norm of the regularized solution $\|F_C(\varepsilon)\|$ is plotted as a function of the residual norm $\|HF(\varepsilon) - Y\|$ in log-log scale. Optimal values of ε lay at the "corner" of the typical L-shaped plot obtained.

However, in this work we decided to use the availability of two identification results—respectively from the motion responses at x_1 and x_2—to estimate the optimal values of the regularization parameters ε_1 and ε_2. These were obtained at the minimum of the norm of the difference between the two force estimates, scaled by a norm related to their amplitude. For instance, looking at the contact force identifications at x_C based on the response accelerations at locations x_1 and x_2, we have the following error function to be minimized by the optimal regularization parameters ε_1 and ε_2:

$$\text{Error}(\varepsilon_1^a, \varepsilon_2^a) = \frac{\|F_C(\omega; \varepsilon_1^a) - F_C(\omega; \varepsilon_2^a)\|}{\|F_C(\omega; \varepsilon_1^a) + F_C(\omega; \varepsilon_2^a)\|}$$

$$\text{with} \quad F_C(\omega; \varepsilon_R^a) = \frac{A(x_R, \omega)}{H_{\text{REG}}^a(x_C, x_R, \omega; \varepsilon_R^a)} \quad (R = 1, 2) \quad (15)$$

As illustrated in Fig. 9, minimization of this function is achieved using parameters $\varepsilon_1^a = 0.985$ and $\varepsilon_2^a = 1.63$, which lead to an optimal regularization. The identifications of the impact force thus obtained, shown in Fig. 10, are clearly less noisy and reasonably faithful to the true result.

The tube motion at the support location may be easily estimated from the previous equations. Indeed, from Eq. (10) we obtain

$$Y(x_C, \omega) = H(x_C, x_C, \omega) F_C(\omega) = H(x_C, x_C, \omega) \frac{Y(x_R, \omega)}{H(x_C, x_R, \omega)} \quad (16)$$

Then, the motion at the support may be directly obtained as

$$Y(x_C, \omega) = G(x_C, x_R, \omega) Y(x_R, \omega) \quad (17)$$

with the transfer function

$$G(x_C, x_R, \omega) = \frac{H(x_C, x_C, \omega)}{H(x_C, x_R, \omega)} \quad (18)$$

Figure 11 shows, beyond the real displacement $Y_C(t)$ at the gap-support x_C, the displacement identifications at the same location, $Y_{1,2}^a(t)$, $Y_{1,2}^v(t)$, and $Y_{1,2}^d(t)$, obtained respectively from $A_{1,2}(t)$, $V_{1,2}(t)$, and $D_{1,2}(t)$. These identification results are most satisfying. Notice that the real and identified beam response traces, at the gap-support, are almost identical. On the other hand, the identified impacts shown in Fig. 10 and the bounded gap-response shown in Fig. 11 clearly suggest that the support gap must be about

± 1 mm (in fact, because of the finite value of the support stiffness, the actual beam displacement will be slightly larger than the support gap).

5 A Tentative Approach to Deal With the Turbulent Field Perturbation

We now turn to the second configuration computations, which—as far as the identification problem is concerned—lead to additional difficulties. Figures 12 and 13 show the identified contact force and displacement at the support location, when a preload is applied. As a result of the permanent tube/support contact, the dynamical reaction force is significantly lower than the spiky force obtained in the case of the gap-supported configuration (a). Also, the vibratory motion at the support location is more than one order of magnitude lower than in the gap-supported case.

As a consequence, the identification results for configuration (b) are more sensitive to the perturbing effects of the unmeasured turbulence excitation. Nevertheless, notice that the orders of magnitude of the force and displacement identifications are correct, which for practical purposes may still be acceptable. The contact force estimates shown in Fig. 12 display many features of the real
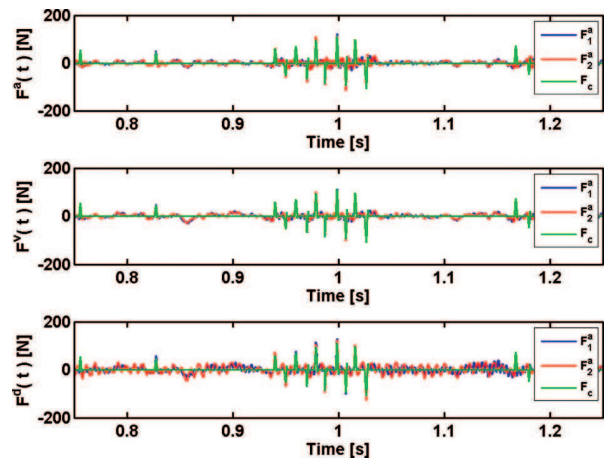

Fig. 10 Regularized impact force identification for the gap-support configuration (a)
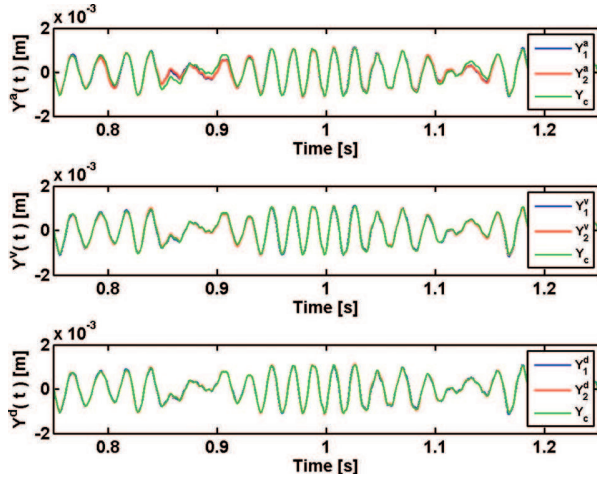
Fig. 11 Regularized identification of the tube motion at the support location for the gap-support configuration (a)
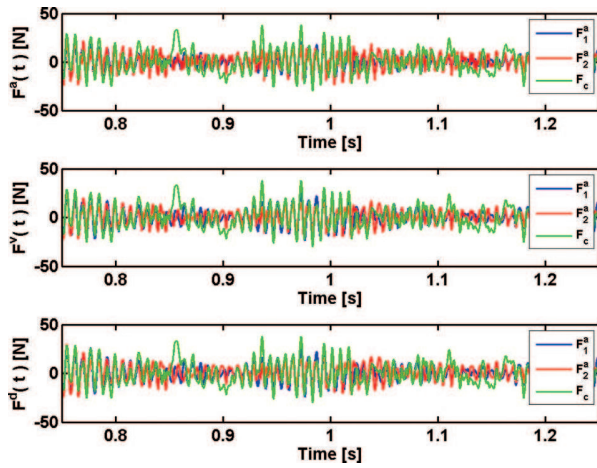

Fig. 12 Regularized impact force identification for preload configuration (b)
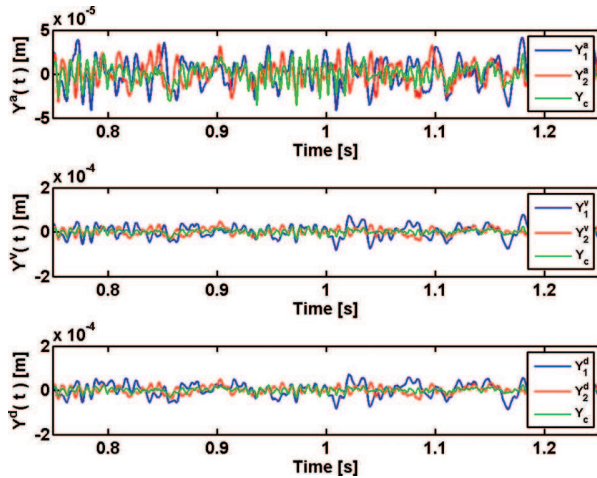

Fig. 13 Regularized identification of the tube motion at the support location for preload configuration (b)

support reaction. However, the amplitudes of the tube motion identifications at the support location, shown in Fig. 13, are over-estimated and their details are totally erroneous.

In order to try to correct somewhat the degrading effects of the unmeasured turbulence excitation, notice that, if the random excitation was applied at a single point x_T, we would have the following response (in the frequency domain), at any given location x_R:

$$Y(x_R,\omega) = H(x_C,x_R,\omega)F_C(\omega) + H(x_T,x_R,\omega)F_T(\omega) \quad (19)$$

Then, we might use the two response measurements $y(x_1,t)$ and $y(x_2,t)$ to build the system

$$Y(x_1,\omega) = H(x_C,x_1,\omega)F_C(\omega) + H(x_T,x_1,\omega)F_T(\omega)$$

$$Y(x_2,\omega) = H(x_C,x_2,\omega)F_C(\omega) + H(x_T,x_2,\omega)F_T(\omega) \quad (20)$$

which would enable the identification of both excitation sources

$$\begin{Bmatrix} F_C(\omega) \\ F_T(\omega) \end{Bmatrix} = \begin{bmatrix} H(x_C,x_1,\omega) & H(x_T,x_1,\omega) \\ H(x_C,x_2,\omega) & H(x_T,x_2,\omega) \end{bmatrix}^{-1} \begin{Bmatrix} Y(x_1,\omega) \\ Y(x_2,\omega) \end{Bmatrix} \quad (21)$$

However, the problem is not so immediate, because the turbulence excitation is distributed along the tube in a complex manner, and no transfer functions $H(x_T,x_R,\omega)$ can be defined. Even so, for the distributed random excitation, we may write Eq. (19) as

$$Y(x_R,\omega) = H(x_C,x_R,\omega)F_C(\omega) + \sum_{n=1}^{N} \frac{F_n^T(\omega)\varphi_n(x_R)}{m_n[\omega_n^2 - \omega^2 + 2i\omega\omega_n\zeta_n]} \quad (22)$$

where $F_n^T(\omega)$ stands for the Fourier transform of the modal forces related to turbulence $f_n^T(t)$, as defined in Eq. (4).

Now, the correct Eq. (22) is quite different from Eq. (19). However, it is tempting to simplify this formulation in the following manner:

$$Y(x_R,\omega) \approx H(x_C,x_R,\omega)F_C(\omega) + F_{EQ}^T(\omega)\sum_{n=1}^{N} \frac{\varphi_n(x_R)}{m_n[\omega_n^2 - \omega^2 + 2i\omega\omega_n\zeta_n]} \quad (23)$$

on the basis that, although modal forces $F_n^T(\omega)$ are clearly different—so, strictly speaking, they cannot be taken out of the summation in Eq. (22)—each modal force is essentially effective only within the frequency range of the corresponding tube mode. This assumption should be realistic, provided the modal frequencies are sufficiently separate and the modal damping is low. Then the "equivalent" turbulence force $F_{EQ}^T(\omega)$ stands for *all* modal forces $F_n^T(\omega)$, each one being dominant in the frequency range $\omega_n - 0.5\Delta\omega_{n-1} \leq \omega \leq \omega_n + 0.5\Delta\omega_{n+1}$, where $\Delta\omega_{n-1} \approx \omega_n - \omega_{n-1}$ and $\Delta\omega_{n+1} \approx \omega_{n+1} - \omega_n$.

From the previous discussion, we can write the following formulation to account for the turbulence excitation in an approximate manner:

$$\begin{Bmatrix} F_C(\omega) \\ F_{EQ}^T(\omega) \end{Bmatrix} = \begin{bmatrix} H(x_C,x_1,\omega) & G(x_1,\omega) \\ H(x_C,x_2,\omega) & G(x_2,\omega) \end{bmatrix}^{-1} \begin{Bmatrix} Y(x_1,\omega) \\ Y(x_2,\omega) \end{Bmatrix} \quad (24)$$

with each $G(x_R,\omega)$ related to turbulence excitation defined as

$$G(x_R,\omega) = \sum_{n=1}^{N} \frac{\varphi_n(x_R)}{m_n[\omega_n^2 - \omega^2 + 2i\omega\omega_n\zeta_n]} \quad (25)$$

Before showing some identification results obtained using formulation (24) and (25), some more comments on the problem regularization should be added. Noise amplification will arise at frequencies where the transformation matrix
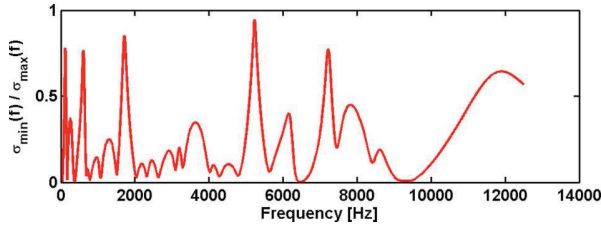
Journal of Pressure Vessel Technology

Fig. 14 Inverse condition number for the transformation matrices $[M^a(\omega)]$, $[M^v(\omega)]$, and $[M^d(\omega)]$

$$[M(\omega)] \equiv \begin{bmatrix} H(x_C, x_1, \omega) & G(x_1, \omega) \\ H(x_C, x_2, \omega) & G(x_2, \omega) \end{bmatrix} \qquad (26)$$

is near-singular. Among the various techniques that can be used to mitigate the problem, filtering by SVD decomposition of $[M(\omega)]$ appears as very elegant and effective. Singularity of a given matrix can be quantified through the so-called *condition number*, which is the ratio between the highest and the lowest singular values of the SVD decomposition

$$[M(\omega)] = [U(\omega)][\Sigma(\omega)][V(\omega)]^T = \sum_{m=1}^{M} \sigma_m(\omega)\{u_m(\omega)\}\{v_m(\omega)\}^T$$

$$(27)$$

with $\sigma_1 \ge \sigma_2 \ge \ldots \ge 0$. Then $C(\omega) = \sigma_{max}/\sigma_{min} = \sigma_1/\sigma_M$, the matrix being perfectly conditioned when $C = 1$ and ill conditioned as C increases. We tend to prefer the use of the inverse quantity $S = 1/C$ because it nicely normalizes in the range $0 \le S \le 1$, with $S = 1$ for perfectly conditioned matrices and $S = 0$ for singularity. Figure 14 illustrates how $S(\omega)$ behaves for the present problem, the plot being identical for acceleration, velocity, and displacement transformation matrices

$$[M^v(\omega)] = i\omega[M^d(\omega)], \quad [M^a(\omega)] = -\omega^2[M^d(\omega)] \qquad (28)$$

The inverse transformation can be computed from the SVD terms as

$$[M(\omega)]^{-1} = [V(\omega)][\Sigma(\omega)]^{-1}[U(\omega)]^T = \sum_{m=1}^{M} \frac{1}{\sigma_m(\omega)}\{v_m(\omega)\}\{u_m(\omega)\}^T$$

$$(29)$$

And typically SVD regularization consists on neglecting all terms such that $S(\omega) < \varepsilon$. Then, Eq. (27) becomes

$$[M^{REG}(\omega)]^{-1} \approx \sum_{m=1}^{P} \frac{1}{\sigma_m(\omega)}\{v_m(\omega)\}\{u_m(\omega)\}^T \qquad (30)$$

with $P \le M$. Actually, because the sensitivity to noise of the acceleration, velocity, and displacement signals is quite different, we have found useful to base the regularization procedure, not on $S(\omega)$, but on the modified quantifier

$$\hat{S}(\omega) = \frac{\sigma_{min}(\omega)}{\sigma_{MAX}} \quad \text{with} \quad \sigma_{MAX} = \max_{0 \le \omega \le \omega_{max}} [\sigma_{max}(\omega)] \qquad (31)$$

which is shown in Fig. 15 for the various transformation matrices. One may notice that the filtering frequency range will be much more severe for $[M^d(\omega)]$ than for $[M^a(\omega)]$, which is reasonable because most high-frequency information in displacement signals is not relevant. The regularization of the velocity transformation $[M^v(\omega)]$ lays in-between the two mentioned extreme cases.

Notice that the definition (31) is less artificial than it seems, because such would be the weighing of the (many) singular values obtained if all the spectral terms were assembled in a single large band-matrix, instead of being processed frequency per frequency

$$[M_{TOT}] \equiv \begin{bmatrix} [M(\omega_1)] & [0] & \cdots & [0] \\ [0] & [M(\omega_2)] & \cdots & [0] \\ \vdots & \vdots & \ddots & \vdots \\ [0] & [0] & \cdots & [M(\omega_{max})] \end{bmatrix} \qquad (32)$$

Such procedure, while mathematically equivalent, would obviously entail a useless waste of computer resources; however, it suggests why the filtering criterion applied to definition (31) seems adequate.

The above-mentioned identification method was first applied to the signals of the gap-support configuration (a). The results, shown in Figs. 16 and 17, are cleaner than those obtained without the correction for the turbulence excitation. However, it is with the preload configuration (b) that a significant improvement is found in the identification results, as attested by Figs. 18 and 19. A better correlation is now found between the identified and the real force signals, and adequate results are now obtained for identification of the tube response at the support location. The proposed correction technique seems therefore effective.

6 Effects of Errors in the Modal Basis Used for Identification

Up to this point, all identifications were performed by building the transfer functions (11)–(13) and (18) with the exact modal
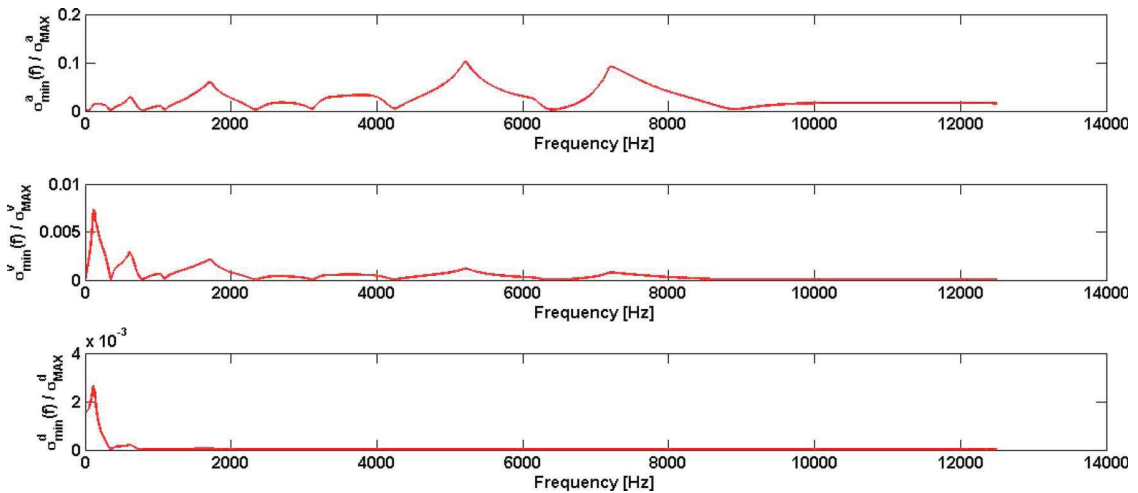

Fig. 15 Global inverse condition numbers for the transformation matrices $[M^a(\omega)]$, $[M^v(\omega)]$, and $[M^d(\omega)]$
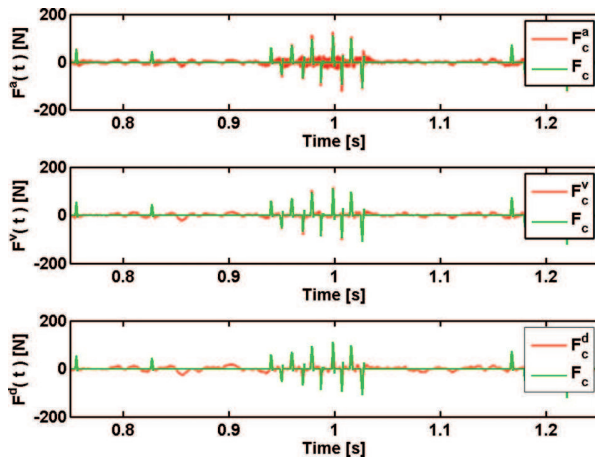
Fig. 16 Turbulence-corrected impact force identification for the gap-support configuration (a)

Fig. 19 Turbulence-corrected identification of the tube motion at the support location for preload configuration (b)
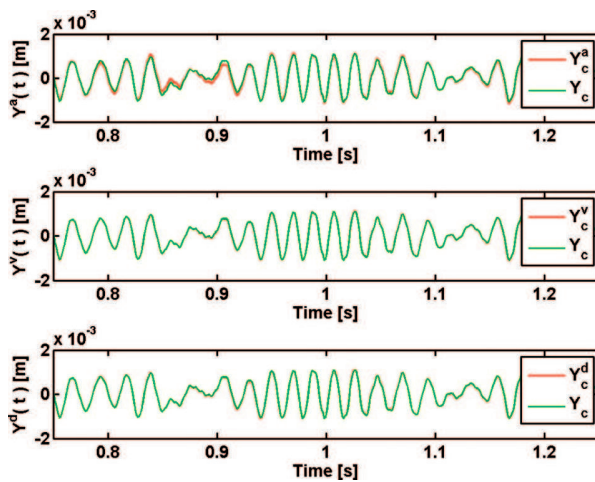

Fig. 17 Turbulence-corrected identification of the tube motion at the support location for the gap-support configuration (a)
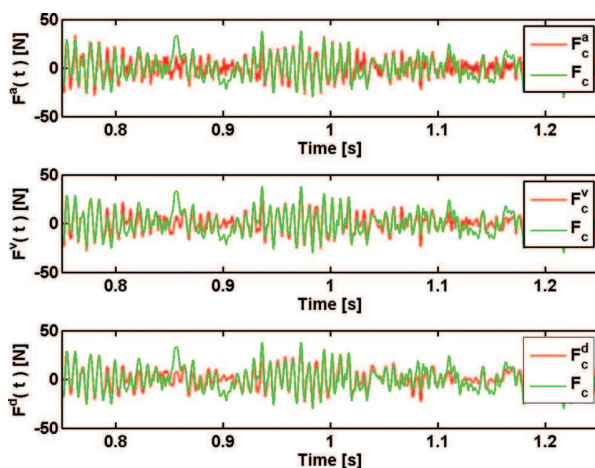

Fig. 18 Turbulence-corrected impact force identification for preload configuration (b)
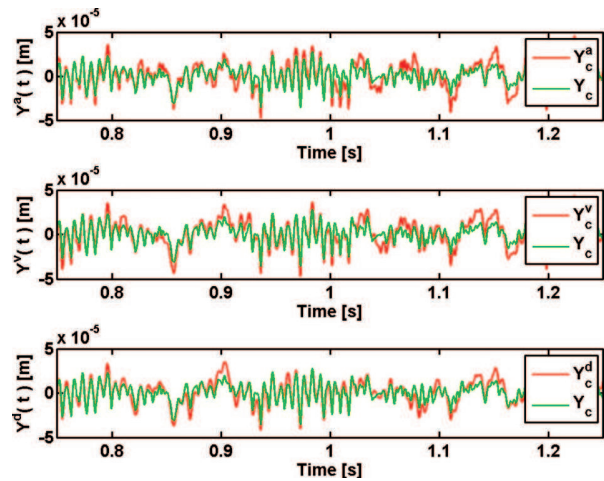
parameters (unconstrained at the nonlinear supports) which were previously used for computing the time-domain nonlinear system responses. This is obviously nonrealistic, because in practice the modal parameters used for identification purposes will always be polluted by some random errors, connected with the less-than-perfect knowledge of the system modes. Because the identification errors induced by the use of nonexact modal parameters may sometimes be catastrophic—see Refs. [32,33], where this issue is thoroughly discussed—it proves essential to investigate if such is the case for the problem addressed in the present paper.

Therefore we will perform in the present section the identification of the impact forces $F_C(t)$ and beam responses $Y_C(t)$, for the two basic cases shown in Figs. 1(a) and 1(b), while introducing realistic random perturbations on all modal parameters of the identification modal basis. These are generated by sampling a uniform distribution rand[0,1], so that each modal parameter p_n is perturbed in the range $p_n/(1+\Delta p_n) \leq p_n^{\text{pert}} \leq p_n(1+\Delta p_n)$. Then,

$$p_n^{\text{pert}} = p_n \left\{ \frac{1 + \Delta p_n(2 + \Delta p_n)\text{rand}[0,1]}{1 + \Delta p_n} \right\} \quad (33)$$

We are conscious that a random distribution generated using this approach is biased, in the sense that its average value is weakly different from the nominal value p_n. Nevertheless, we decided to do so, in order to be able to apply severe random perturbations to the modal damping coefficients without getting nonphysical negative values. Furthermore, when the random perturbations are small, we have $p_n/(1+\Delta p_n) \approx p_n(1-\Delta p_n)$ leading to a nearly centered distribution.

The following maximum values for the random errors were adopted here: modal masses $\Delta m_n = \pm 10\%$, modal frequencies $\Delta \omega_n = \pm 5\%$, modal damping $\Delta \zeta_n = \pm 100\%$, and modeshapes $\Delta \varphi_n(x_C) = \Delta \varphi_n(x_1) = \Delta \varphi_n(x_2) = \pm 10\%$. We reckon these upper bounds to be realistic, for instance, when the modal parameters are obtained from an experimental modal identification. Figure 20 shows the actual random errors which were simultaneously applied to all the modal parameters, leading to the identification results presented in Figs. 21 and 22.

Figure 21 shows the main results obtained for configuration (a). Here, for compactness, only are shown the identifications of $F_C(t)$ and $Y_C(t)$, computed by processing the remote acceleration responses through the perturbed transfer functions. When compared with the corresponding results obtained using the exact modes, see the upper plots of Figs. 16 and 17, one can only notice a slight deterioration in the identified beam displacement at the gap-support. Figure 22 presents the identifications obtained for the
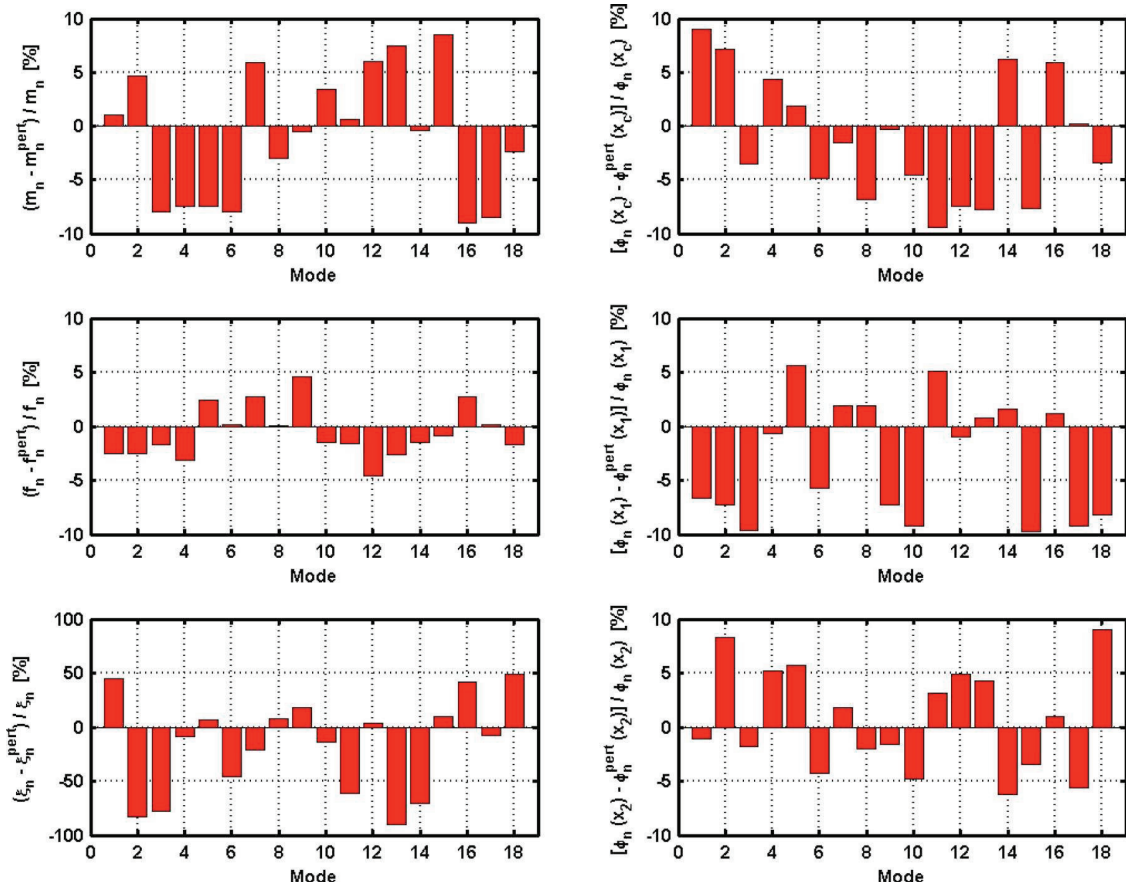
Fig. 20 Random error perturbations applied to the modal parameters used for the identifications

harder problem posed by configuration (b). A comparison with the upper plots of Figs. 18 and 19 reveals some differences, but it would be hazardous to state that the results of Fig. 22 are worse than those obtained using the exact modes. Indeed, such differences are not particularly significant, when compared with the residual perturbations from the unmeasured turbulence excitation.

Therefore, it can be concluded that for the system addressed in this paper, a realistic amount of incertitude in the modal basis used for identification will not lead to a catastrophic deterioration of the identified forces and vibratory responses, which remain in all cases usable.

7 Conclusions

In this paper, we addressed the important topic of remote identification of contact/impact forces and tube motions at gap-supports and preloaded supports. Attention was paid to regularization techniques, two of them—a variant of Tikhonov regularization and SVD filtering—being explored and discussed in detail. The illustrative identification results presented in the paper highlight the importance of noise pollution effects, and hence the need for regularization procedures.

The main contribution of the paper is a proposed corrective identification technique, using a couple (or more) response measurements, which proved effective in reducing the perturbing ef-
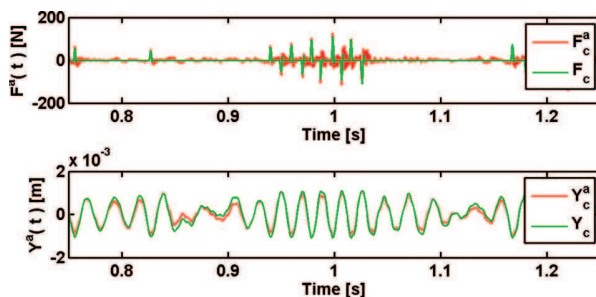

Fig. 21 Effect of random errors in the modal parameters used for the identifications at the gap-support configuration (a). Turbulence-corrected identifications of the impact force and of the tube motion at the support location (identifications performed from the remote acceleration responses).
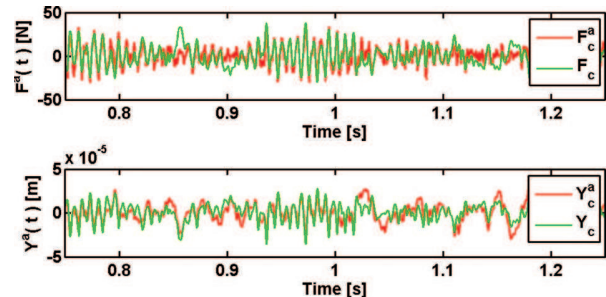

Fig. 22 Effect of random errors in the modal parameters used for the identifications at the gap-support configuration (b). Turbulence-corrected identifications of the impact force and of the tube motion at the support location (identifications performed from the remote acceleration responses).

fects of the unmeasured distributed turbulence excitation. Overall, the combined use of the various techniques discussed enabled quite satisfying identifications, even under difficult conditions. The spiky forces connected with impacts at gap-supports, and the corresponding tube responses, are easier to identify than the continuous random support forces obtained under preload conditions. Understandably, signals issued by displacement transducers are better suited to identify the tube responses than the contact/impact forces. Velocity and acceleration transducers provide signals, which are more adequate for such purposes.

Finally, we investigated the effects of random perturbations of the modal parameters used for performing the identifications. The results obtained show that, for the problem addressed in this paper, the identification results remain sufficiently accurate when realistic errors are introduced in the modal parameters.

We are currently extending the present work to two-dimensional motions and—which entails new difficulties—to deal with multisupported tubes. Also, experiments are being prepared, in order to validate the discussed identification techniques.

Nomenclature

A	=	area of the beam cross section
D	=	tube diameter
e	=	tube wall thickness
E	=	Young's modulus of the tube
$f_T(x,t)$	=	distributed turbulence force field
$F_C(t)$	=	contact/impact force at support
f	=	frequency
$f_R = fD/\bar{V}_f$	=	dimensionless frequency
$f_n(t)$	=	modal force
$\mathcal{F}[\dots]$	=	Fourier transform
$\mathcal{F}^{-1}[\dots]$	=	inverse Fourier transform
$H(\omega)$	=	generic transfer matrix
I	=	moment of inertia of the tube cross section
$k(\omega)$	=	dispersion equation
K_C	=	tube/support contact stiffness
L	=	tube length
m_n	=	modal mass
$n = 1,2,\dots,N$	=	modal index
$q_n(t)$	=	modal response
t	=	time
x	=	generic location along the tube
x_1, x_2	=	locations of transducers 1 and 2 where vibratory responses are sensed
x_C	=	location of the gap support
$y(x,t)$	=	flexural tube response
ρ	=	mass density of the tube
η	=	tube viscous dissipation coefficient
δ_C	=	support gap
ω_n	=	modal circular frequency
ζ_n	=	modal damping
$\varphi_n(x)$	=	modeshape

References

[1] Rogers, R. J., and Pick, R., 1977, "Factors Associated With Support Forces Due to Heat Exchanger Tube Vibration Contact," Nucl. Eng. Des., **44**, pp. 247–253.

[2] Axisa, F., Antunes, J., and Villard, B., 1988, "Overview of Numerical Methods for Predicting Flow-Induced Vibrations," ASME J. Pressure Vessel Technol., **110**, pp. 7–14.

[3] Antunes, J., Axisa, F., Beaufils, B., and Guilbaud, D., 1990, "Coulomb Friction Modelling in Numerical Simulations of Vibration and Wear Work Rate of Multi-Span Heat-Exchangers," J. Fluids Struct., **4**, pp. 287–304.

[4] Axisa, F., Antunes, J., and Villard, B., 1990, "Random Excitation of Heat-Exchanger Tubes by Cross-Flow," J. Fluids Struct., **4**, pp. 321–341.

[5] Fricker, A., 1991, "Vibro-Impact Behaviour of Fluid-Elastically Unstable Heat Exchanger Tubes With Support Clearances," International Conference on Flow-Induced Vibrations, Institute of Mechanical Engineers, Brighton, UK, pp. 129–137.

[6] Sauvé, R. G., 1996, "A Computational Time Domain Approach to Fluidelastic Instability for Nonlinear Tube Dynamics," ASME Paper No. ASME PVP-328.

[7] Yetisir, M., and Fisher, N., 1996, "Fretting-Wear Prediction in Heat Exchanger Tubes: The Effect of Chemical Cleaning and Modelling Ill-Defined Support Conditions," ASME Paper No. ASME PVP-328.

[8] Antunes, J., Axisa, F., and Vento, M., 1992, "Experiments on Tube/Support Interaction with Feedback-Controlled Instability," ASME J. Pressure Vessel Technol., **114**, pp. 23–32.

[9] Boucher, K., and Taylor, C., 1996, "Tube Support Effectiveness and Wear Damage Assessment in the U-Bend Region of Nuclear Steam Generators," ASME Paper No. ASME PVP-328.

[10] Fisher, N., Tromp, J., and Smith, B., 1996, "Measurement of Dynamic Interaction Between a Vibrating Fuel Element and Its Support," ASME Paper No. ASME PVP-328.

[11] Mureithi, N., Ito, T., and Nakamura, T., 1996, "Identification of Fluidelastic Instability Under Conditions of Turbulence and Nonlinear Tube Supports," ASME Paper No. ASME PVP-328.

[12] Vento, M. A., Antunes, J., and Axisa, F., 1992, "Tube/Support Interaction Under Simulated Fluidelastic Instability: Two-Dimensional Experiments and Computations of the Nonlinear Responses of a Straight Tube," ASME Paper No. ASME PVP-242.

[13] Whiston, G. S., 1984, "Remote Impact Analysis by Use of Propagated Acceleration Signals: I-Theoretical Methods," J. Sound Vib., **97**, pp. 35–51.

[14] Jordan, R. W., and Whiston, G. S., 1984, "Remote Impact Analysis by Use of Propagated Acceleration Signals: II–Comparison Between Theory and Experiments," J. Sound Vib., **97**, pp. 53–63.

[15] Doyle, J., 1989, *Wave Propagation in Structures: An FFT-Based Spectral Analysis Methodology*, Springer-Verlag, New-York.

[16] De Araújo, M., Antunes, J., and Piteau, P., 1998, "Remote Identification of Impact Forces on Loosely Supported Tubes: Part 1—Basic Theory and Experiments," J. Sound Vib., **215**, pp. 1015–1041.

[17] Antunes, J., Paulino, M., and Piteau, P., 1998, "Remote Identification of Impact Forces on Loosely Supported Tubes: Part 2–Complex Vibro-Impact Motions," J. Sound Vib., **215**, pp. 1043–1064.

[18] Paulino, M., Antunes, J., and Izquierdo, P., 1999, "Remote Identification of Impact Forces on Loosely Supported Tubes: Analysis of Multi-Supported Systems," ASME J. Pressure Vessel Technol., **121**, pp. 61–70.

[19] Lin, S. Q., and Bapat, C. N., 1992, "Estimation of Clearances and Impact Forces Using Vibroimpact Response: Sinusoidal Excitation," J. Sound Vib., **157**, pp. 485–513.

[20] Lin, S. Q., and Bapat, C. N., 1993, "Estimation of Clearances and Impact Forces Using Vibroimpact Response: Random Excitation," J. Sound Vib., **163**, pp. 407–421.

[21] Lin, S. Q., and Bapat, C. N., 1993, "Extension of Clearance and Impact Force Estimation Approaches to a Beam-Stop System," J. Sound Vib., **163**, pp. 423–428.

[22] Busby, H. R., and Trujillo, D. M., 1987, "Solution of an Inverse Dynamics Problem Using an Eigenvalue Reduction Technique," Comput. Struct., **25**, pp. 109–117.

[23] Wu, E., and Yeh, J. C., 1994, "Identification of Impact Forces at Multiple Locations on Laminated Plates," AIAA J., **32**, pp. 2433–2439.

[24] Kim, J. T., and Lyon, R. H., 1992, "Cepstral Analysis as a Tool for Robust Processing, Deverberation and Detection of Transients," Mech. Syst. Signal Process., **6**, pp. 1–15.

[25] Inoue, H., Harrigan, J. J., and Reid, S. R., 2001, "Review of Inverse Analysis for Indirect Measurement of Impact Force," Appl. Mech. Rev., **54**(6), pp. 503–524.

[26] Jeffrey, W., and Rosner, R., 1986, "On Strategies for Inverting Remote Sensing Data," Astrophys. J., **310**, pp. 463–472.

[27] Dimri, V., 1992, *Deconvolution and Inverse Theory: Application to Geophysical Problems*, Elsevier, Amsterdam.

[28] Parker, R. L., 1994, *Geophysical Inverse Theory*, Princeton University Press, Princeton, NJ.

[29] Press, W. H., Teukolsky, A. A., Vetterling, W. T., and Flannery, B. P., 1992, *Numerical Recipes: The Art of Scientific Computing*, Cambridge University Press, Cambridge, UK.

[30] Groetch, C. W., 1993, *Inverse Problems in the Mathematical Sciences*, Vieweg, Wiesbaden.

[31] Hansen, P. C., 1994, "Regularization Tools," Numer. Algorithms, **6**, pp. 1–35.

[32] Debut, V., Delaune, X., and Antunes, J., 2009, "Identification of Nonlinear Interaction Forces Acting on Continuous Systems Using Remote Measurements of the Vibratory Responses," Proceedings of the Seventh EUROMECH Solids Mechanics Conference (ESMC2009), Lisbon, Portugal, Sept. 7–11.

[33] Debut, V., Delaune, X., and Antunes, J., 2010, "Identification of the Nonlinear Excitation Force Acting on a Bowed String Using the Dynamical Response at Remote Locations," Int. J. Mech. Sci., in press.

[34] Antunes, J., Delaune, X., Piteau, P., and Borsoi, L., 2008, "A Simple Consistent Method for the Time-Domain Simulation of Turbulence Excitations Applied to Tube/Support Dynamical Analysis Under Non-Uniform Flows," Proceedings of the Ninth International Conference on Flow Induced Vibrations (FIV-2008), Prague, Czech Republic, Jun. 30–Jul. 3.

[35] Antunes, J., Piteau, P., Delaune, X., and Borsoi, L., 2009, "An Evaluation of Methods for the Time-Domain Simulation of Turbulence Excitations for Tube Bundles Subjected to Non-Uniform Flows," Proceedings of the 20th International Conference on Structural Mechanics in Reactor Technology (SMIRT 20), Espoo, Finland, Jun. 9–14.